Water adsorption on hydroxylated silica surfaces studied using the density functional theory

Jianjun Yang, Sheng Meng, Lifang Xu, and E. G. Wang*
Beijing National Laboratory for Condensed Matter Physics and Institute of Physics, Chinese Academy of Sciences, Box 603, Beijing 100080, China

(Received 25 September 2004; revised manuscript received 2 November 2004; published 19 January 2005)

We present an *ab initio* investigation of water adsorption on ordered hydroxylated silica surfaces, using the density functional theory within the ultrasoft pseudopotentials and generalized-gradient approximation. The (100) and (111) surfaces of the hydroxylated cristobalite are used as substrates to adsorb water clusters and overlayers. Water adsorbs through hydrogen bonds formed between water and surface hydroxyl groups on the $\beta(\alpha)$-cristobalite (100) surface. A large enhancement of the hydrogen bonding in the adsorbed water dimer is observed, which can be inferred from the shortened hydrogen-bond (H bond) length, the vibrational spectra from the molecular dynamics simulation and the redistribution of electron density. At one monolayer (ML) coverage, a "tessellation ice," with characteristic quadrangular and octagonal hydrogen-bonded water rings, is formed. It has two types of H bonds and can exist on two different adsorption sites with two different OH orderings in a surface supercell. Our study is further extended to the β-cristobalite (111) surface. Based on these studies, we find that the water-silica bond, which comprises several H bonds, is usually stronger than other associative water-surface interactions. The H bonds between water and surface usually differ in strength—and hence, in vibrational spectra—from those between adsorbed water molecules. Because the (100) and (111) surfaces sustain different silanol groups (geminal and isolated silanols), a well-defined two-dimensional tessellation ice phase can be observed only on the cristobalite (100) surface. On β-cristobalite (111) surface, however, isolated water molecules, hydrogen-bonded to the surface hydroxyls, are formed, even at 1 ML coverage.

DOI: 10.1103/PhysRevB.71.035413 PACS number(s): 68.43.Bc, 82.30.Rs, 68.08.Bc

I. INTRODUCTION

The interaction of water with solid surfaces plays a crucial role in many phenomena, ranging from aqueous heterogeneous chemistry and dissolution of minerals in natural systems to metal corrosion. In particular, the water-silica interface is one of the typical systems that are most frequently encountered in technology and natural materials. Considerable efforts have been dedicated to its study for more than three decades. The numerous technological applications of amorphous silica were found to rely on its specific surface properties.[1,2] A freshly formed amorphous silica will include a distribution of reactive sites, which are known to react rapidly with atmospheric moisture, leading to the formation of surface silanol (Si-OH) groups.[1,2] The reactive chemical and physical properties of the hydroxyl groups on the silica surface are, by and large, responsible for the widespread utility of these materials. Understanding the nature of reactive surface sites available for physisorption and chemisorption of gas phase molecules is crucial to study the behavior of silica for a wide range of applications.[1]

As water vapor inevitably exists in the atmosphere and readily adsorbs on the hydrophilic surface, and the interfacial water structure has significant effects in various processes, such as silica formation and weathering, the interaction of water with silica has been the subject of a wide range of investigations. Various techniques have been used to study water/silica interfaces experimentally in recent years, such as vibrational spectroscopies at quartz/water interfaces,[3] microcalorimetric measurements of water vapor-silica surfaces interactions,[4] and dehydroxylation studies on silica.[5–9] However, due to the vibrational-spectra overlap of OH modes in Si-OH with water, a clear picture of interfacial water structure at the molecular level is hard to achieve. The poverty of experimental evidence particularly evokes interest in the present studies by computational methods. Many theoretical works were carried out, such as on the interaction of water with silica hydroxyls using a cluster model of silanol molecules,[10,11] and with vitreous silica.[12] To our knowledge, except for the work by de Leeuw on water interactions with α-quartz surfaces,[13] few theoretical studies of the interaction between water and crystalline silica surfaces have been performed.

At the same time, a detailed microscopic description of the substrate—the hydroxylated silica surface is still lacking. Existing experimental data on the amorphous hydroxylated surface are often rationalized by modeling the surface as an alternation of patches of the hydroxylated (100) and (111) surfaces of β-cristobalite, which is the crystalline phase of silica with density and refractive index closest to those of amorphous silica.[2,14] Moreover, the two main faces of β-cristobalite can sustain the two types of hydroxyl groups identified experimentally on the amorphous silica surface, namely, the single silanols (Si-OH) of the (111) surface, and the geminal silanols [Si-$(OH)_2$], which are typical on the (100) surface. A lot of previous works investigating silica surfaces have been performed based on this model,[14–17] such as the works on the dehydroxylation of the silica surfaces by Iarlori and Ceresoli *et al.*[15,16] In a recent letter,[18] we proposed a two-dimensional (2D) ice phase on the hydroxylated β-cristobalite(100) surface at monolayer (ML) coverage—which had not been found on other surfaces or in bulk ice

before—by using *ab initio* calculations based on the density functional theory (DFT). In this phase water forms an ordered 2D quadrangular and octagonal hydrogen-bond (H-bond or HB) network. Further molecular dynamics (MD) simulations show that this tessellation ice is stable up to room temperature.

In order to give a more complete picture for water adsorption on a silica surface we extend our first-principles study to more general cases. In the present paper, various water adsorption species on the two typical hydroxylated β-cristobalite surfaces, (100) and (111), which sustains two types of silanols identified experimentally on silica surfaces, have been studied. Another relevant silica surface, α-cristobalite (100), which is a low temperature counterpart of β-cristobalite (100), is also investigated. These crystalline surfaces not only have their own interests to interact with water, but also represent the applicable models of the small domains on the amorphous silica surface.

We first studied a water monomer adsorption on β-cristobalite (100) in detail, which can provide us a fundamental picture and a start point of the interaction between water and the silica surface. The adsorption of water dimers is another interesting issue because the H bonds in both water-water and water-surface interactions are involved in this system. It was found that the H bonding interaction in a dimer is largely strengthened upon adsorption, as was also confirmed by vibrational analysis and electron transfer along H bonds. We further studied the stable configurations at half water monolayer. It shows that before 1 ML is reached, adsorbed water always exists as isolated clusters. More detailed studies have been carried out at monolayer coverage, where we find the tessellation ice with characteristic quadrangular and octagonal water rings can adsorb on different adsorption sites and in different proton orderings. Our MD simulations of water dimers and monolayer structures demonstrate a strong H-bond interaction in the adsorbed dimers, and two types of H bonds of different strengths in tessellation ice. We note here the present investigation of the effects of different silica surfaces is interesting in its own aspect. As β-cristobalite is the high temperature phase of α-cristobalite, adsorption on α-cristobalite is more realistic to carry out in laboratories at room temperature. However, not much difference was found in our calculations. The ice tessellation also exists perfectly on the α-cristobalite (100) surface, which provides much convenience for future experimental tests.

As mentioned before, the β-cristobalite (111) surface is another important surface, which supports the typical type of silanols—single silanols. It is thus essential to investigate water adsorption onto this surface towards understanding the general feature of water/silica interface. As prototype water adsorption structures, water monomer and monolayer have been calculated on this surface. Our study shows that water molecules behave very differently on the single silanols of β-cristobalite (111) surfaces compared with their behavior on geminal hydroxyl groups of cristobalite (100), as the single, isolated silanol groups do not interact with each other by H bonding.

The outline of this paper is as follows. After the introduction section, we describe in Sec. II detailed computational methods and the theoretical models. The results obtained for different water structures and on several silica surfaces are presented and discussed in Sec. III. In Sec. IV we analyze their vibrational spectra and electronic properties. And finally a summary is given in Sec. V.

II. COMPUTATIONAL DETAILS

We have carried out a systematic *ab initio* density functional theory study of water adsorption on silica surfaces. All the calculations have been carried out using the VASP code (Vienna *ab initio* simulation package),[19] an efficient plane-wave implementation of density functional theory, which enables us to do both structure optimizations and molecular dynamics simulations and has been extensively reviewed elsewhere.[20] Other than the classical simulations based on empirical water-surface potentials, which are usually inadequate to quantitatively describe the interface properties, *ab initio* calculations based on the DFT can provide a valuable insight into the nature of water-solid interaction and aids in the identification of the reactive surface sites for the hydration and dehydration processes. The generalized gradient approximation (GGA) by Perdew and Wang (PW91)[21] is used for the exchange correlation energy, which has been shown to give reliable results for the energetics of adsorbates; e.g., water on TiO_2 and SnO_2 (Ref. 22), and CaO.[23] The GGA extension is crucial for the accurate treatment of the hydrogen bonds and water structures.[24] The PW91 form has been tested extensively for a variety of intermolecular interactions including H bonding.[25] Within the pseudopotential approach, only the valence electrons are treated explicitly, and the pseudopotential represents the effective interaction of the valence electrons with the atomic cores. The valence orbitals are expanded in a plane-wave basis set. Relatively high plane-wave energy cutoffs have to be used when studying elements such as oxygen, which has tightly bound $2p$ electrons. The VASP program employs Vanderbilt ultrasoft pseudopotentials (USPP),[26] which can mitigate the requirement of large basis set of plane-wave calculations for a given accuracy.

Kohn-Sham orbits are expanded in plane waves up to a kinetic energy cutoff of 350 eV for most of the calculations presented in this paper. The Monkhorst-Pack scheme[27] with $4\times4\times4$ and $2\times2\times1$ k-points grid mesh has been used for integration in the bulk and surface Brillouin zone (BZ), respectively. The geometry optimization is stopped when energy convergence is less than 0.0001 eV per atom. First we modeled β-cristobalite in a cubic supercell containing eight formula units. Within this scheme we found the optimized internal structural parameters of bulk are 150.9° (SiOSi), 109.4° and 110.2° (OSiO), and 1.612 Å (Si-O) in excellent agreement with the experimental values 146.7°, 107.8°, and 112.8°, and 1.611 Å[28] and with previous local density approximation (LDA) calculation using Troullier-Martins norm-conserving pseudopotentials[15] and the Hartree-Fock calculation.[29] To model the surface, we used the usual approach by considering a supercell that contains the slab geometry with three-dimensional periodic boundary conditions. The slabs are 7–9 atomic layers thick and separated by a vacuum $\sim$10 Å wide. Theoretical lattice constants deter-

mined from bulk calculations—7.21 Å for β-cristobalite and 5.142 Å for α-cristobalite (7.16 and 4.978 Å in experiment)—were used throughout this work.

Before considering water adsorption, we first studied the clean SiO_2 surfaces. Both the surfaces of the silica slab are saturated with hydrogen atoms, and one of them is used to represent the fully hydroxylated surface. In all calculations, all the hydrogen and oxygen atoms in the bottom two layers have been kept fixed at their equilibrium positions, while all the other atoms are allowed to relax freely. We thus obtained the geometry of the completely hydroxylated surfaces by optimizing the structural coordinates. As given in Ref. 18, the optimized geometry of the hydroxylated β-cristobalite (100) surface is covered with geminal and vicinally hydrogen-bonded hydroxyl groups, in good agreement with previous theoretical works.[15,17] The H-bond chains are arrayed in the [110] direction. The H-bond lengths (O-O distance) are 2.63–2.66 Å, suggesting a strong H bonding. There are two geminal silanols in our surface unit cell. Although they are not completely equivalent to each other due to the slight difference in the positions of Si atoms in the surface layer, there is no qualitative difference in the structure by means of accepting and donating one H bond each. The α-phase of cristobalite (100) has a very similar structure, but all the Si atoms are equivalent in the surface layer. In contrast, the hexagonal hydroxylated β-cristobalite (111) surface sustains the other type of silanols, isolated single silanols, which are apart from each other by about 5 Å and cannot form H bonds with each other.

In molecular dynamics simulations, the water molecules and atoms in the surface layer were allowed to move according to the forces calculated from the converged electronic structure. A lower energy cutoff of 300 eV for plane-wave basis and time steps of 0.5 and 1 fs were utilized in all MD simulations. To obtain the vibrational spectra, we performed constant-energy MD runs of 3–4 ps to collect statistics, after equilibrating the system for 1 ps. The vibrational spectra were obtained by performing a Fourier transformation of the velocity-velocity autocorrelation function, recorded in our MD trajectories.[30] A shorter time step of 0.25 fs does not change the peak positions or the shape of the vibrational spectra.

The adsorption energy for an adsorbed water structure, E_{ads}, has been defined as the averaged energy difference per water molecule,

$$E_{ads} = (E_{substrate} + n \times E_{H_2O} - E_{(H_2O)_n/substrate})/n. \quad (1)$$

Here $E_{(H_2O)_n/substrate}$ is the total energy of the adsorption system, $E_{substrate}$ and E_{H_2O} are those for the substrate and a free water molecule, respectively, and n is the number of water molecules in the supercell. The adsorption energy with a positive value indicates binding.

III. RESULTS AND DISCUSSION

We investigated the water adsorption structures in different configurations with the DFT total energy calculations by putting gaseous water molecules on the hydroxylated cristobalite (100) and (111) surfaces. In the first part of this section, the optimal hydrated surface structures and the adsorptive energies were studied in detail for a series of selected water species, such as monomers, dimers, half monolayers and monolayers on β-cristobalite (100). Here the coverage is defined as the ratio of the number of adsorbed water molecules to the number of surface hydroxyls. As there are many local minima on the potential surface for these hydrogen-bonded surface complexes, we have used a range of different starting configurations with several water molecule adsorption sites and their different orientations (up to ten in some cases) to ensure, as far as possible, that the final converged configuration is a global rather than a local minimum-energy configuration. The next two parts extend this study to the other two silica surfaces, α-cristobalite (100) and β-cristobalite (111), respectively, where the general features of water adsorption and the effects of different surface silanol types are investigated.

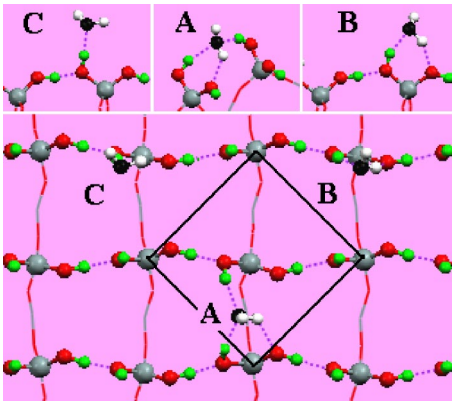

FIG. 1. (Color online) The water monomer adsorbed on the three typical sites of a β-cristobalite (100) surface (top panel for side views, and bottom panel for top views). Three letters A, B, C, label configurations following a sequence of decreasing adsorption energy. The water molecules have been colored with black oxygen and white hydrogen to distinguish from the hydroxyl groups on the surface (colored dark gray and light gray). Black lines depict the surface cell in the calculations.

A. Water adsorption on β-cristobalite (100) surface

1. Water monomer on β-cristobalite (100)

As a starting point towards a general understanding of water-silica bonds, we studied the adsorption of a single water molecule on the hydroxylated β-cristobalite (100) surface first. To find out the exact global energy minimum of the potential energy surface, geometry optimization has been performed on a set of configurations with the water molecule located at typical adsorption sites of the surface, such as top, geminal, vicinal, and bridge sites. The calculated equilibrium structures are shown in Fig. 1, where the bridge, geminal, and top sites are labeled as A, B, and C, respectively, following a sequence of decreasing adsorption energies. The adsorption energies as well as the optimized geometrical parameters of the water adsorbate, determined from calculations in a unit surface cell, are listed in Table I. Our

TABLE I. The calculated geometries and energetics for the monomer adsorption on several typical adsorption sites of β-cristobalite (100). Numbers of H bonds (N_{HB}), adsorption energies (E_{ads} in meV/H_2O), OH bond lengths (d_{OH} in Å) and bond angles ($\angle$HOH in deg) of water molecules, are listed. The adsorption site on which all the OH bonds in the water monomer are H bonded is labeled as bridge2 here. The last row lists the calculated values for a gaseous water molecule for comparison.

	N_{HB}	E_{ads}	d_{OH1}	d_{OH2}	$\angle$HOH
Top	1	339	0.970	0.960	106.12
Geminal	2	508	0.973	0.992	106.03
Vicinal	2	442	0.973	0.987	106.13
Bridge	3	622	0.974	0.988	105.06
Bridge2	4	534	0.985	0.988	100.38
H_2O			0.973	0.973	104.91

calculations show that the adsorption on the bridge site is preferred energetically with the largest adsorption energy of 622 meV/H_2O, where the single water molecule is stabilized by means of three hydrogen bonds [see Fig. 1(A)], acting as the double proton acceptor and a proton donor involved with the surface geminal silanols. Here we assume the hydrogen bond is formed when the O–O bond length is less than 3.30 Å and the O–H···O angle is greater than 140°. One of the OH bonds stands upright, while the other OH bond is almost parallel to the substrate. The adsorption energy on the geminal site is lower by forming only two HBs with the surface [Fig. 1(B)], as can be seen from Table I. Similarly, the adsorption on the vicinal site, above the two H-bonded surface hydroxyls, has almost the same stability as on the geminal site. The top site is the most unfavorable configuration among those we have investigated, with the smallest adsorption energy of 339 meV, and only one HB is formed there [Fig. 1(C)]. However, increasing H bonds to more than three does not enhance the water-surface bonding. For instance, water lying down almost flat on the bridge site forms another HB (denoted as bridge2 in Table I), and consequently it is saturated with four H bonds interacting with the surface hydroxyl groups. This configuration with four H bonds is found to be a metastable with the adsorption energy lowered by ~88 meV than the most stable structure. We thus come to a general conclusion that for water adsorption on the surfaces or interfaces, the adsorption energy does not necessarily increase with the increase of the number of H bonds there formed. Another noteworthy point is that Si-O -H···OH_2 is always a stronger H bond and results in a shorter H-bond length in turn. Briefly, the bridge site is found to be the most reactive for a water monomer adsorption by characterization of the surface structures.

For comparison we also listed the calculated geometric data of a free water molecule, as listed in Table I. There is a significant deformation of the adsorbed water molecule for most adsorption configurations considered here: one of the two OH bonds is lengthened and the HOH angle is enlarged slightly. This effect of water adsorption is also found on other surfaces, such as metal Pt (111),[30,31] oxide TiO_2 (110),[22] etc. The H-bond lengths (O-O) between the water molecule and the surface hydroxyl are typically 2.82–3.04 Å, which is a little longer than that in ice *Ih*(2.76 Å). H_2O can serve as a bridge between the two adjacent H-bond chains of the surface hydroxyl groups, as seen in Fig. 1.

2. Water dimer and 0.5 ML adsorption on β-cristobalite (100)

We then investigated the water dimer, the simplest H-bonding system, adsorbed on the β-cristobalite (100) surface. Several possible structures for the adsorbed dimer at different surface sites were considered. The optimized structure of the most stable configuration identified in our calculations is depicted in Fig. 2. The energetic and geometric configurations for each molecule in the dimer are specified in Table II.

Similar to the monomer adsorption, the water dimer is much preferred to locate at the bridge site too, as shown in Fig. 2. There are four H bonds between the water dimer and the surface hydroxyls and an internal H bond between water molecules, with one free OH bond sticking away from the surface. The adsorption energy is 748 meV per molecule. Thus a dimer is stabilized by 126 meV/H_2O compared with two isolated water monomers located far away from each other on the surface. The extra stabilization can be mainly attributed to hydrogen bonding between water molecules, though the interaction of each water molecule with the surface differs from that for monomer adsorption. We note that the geometry of the adsorbed dimer looks quite similar to its gas phase (see Table II) and the dimer on other surfaces, such as Pt(111)[30,31] and Pd(111),[32] but still exhibits several interesting characteristics in the details. First, the heights of the

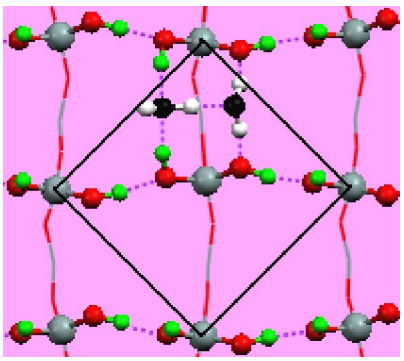

FIG. 2. (Color online) The adsorbed water dimer on β-cristobalite (100).

TABLE II. The adsorption energies and geometries for a water dimer on β-cristobalite (100), and the theoretical and experimental values for a free dimer. Energies, distances, and angles are in units of meV/H_2O, Å, and deg (°), respectively. The adsorption site on which all the OH bonds in the water dimer are H bonded is labeled as bridge2 here. We use the same definition of angles α and β, and OO distances (d_{OO}) to describe the geometry of a water dimer as in Ref. 31. Other geometrical parameters are the same as in Table I.

	E_{ads}	N_{HB}	d_{OH1}	d_{OH2}	∠HOH	d_{OO}	α	β
Geminal	544	3	0.973	1.009	106.32	2.655	9.38	105.65
			0.974	1.005	105.35			
Bridge	748	5	0.973	1.043	108.85	2.530	8.48	103.58
			0.994	0.992	103.63			
Bridge2	650	5	0.981	1.014	104.21	2.671	8.61	98.70
			0.987	0.989	104.22			
Free dimer			0.973	0.984	104.79	2.895	2.79	126.00
			0.973	0.973	105.08			
Dimer(expt.)[a]						2.976	−1±6	123±6

[a]Reference 33.

two water molecules in the adsorbed dimer differ substantially. The H-bond donor molecule lies 0.50 Å closer to the substrate than the H-bond acceptor. Compared to the water monomer, the H-bond donor water is 0.15 Å closer to the surface and interacts more strongly with it, whereas the H-bond acceptor water interacts very weakly with the surface for the farther distance from the surface by 0.35 Å. Similar trends are found in water dimers on Pt(111)[30,31] and Pd(111).[32] Second, if the same definitions of the two angles, α and β, as those in Ref. 31 are used to depict the dimer structure, the donor and acceptor molecules in the adsorbed dimer make an angle β of 104°, much smaller than that in the gas phase dimer and the dimer on metal surfaces (around 126°).[31] Third, the O-O distance in the adsorbed dimer, 2.53 Å, is shortened to a great degree than the equilibrium distance for the gaseous dimer (2.89 Å in our calculation and 2.98 Å in experiment)[33] and adsorbed dimer on metals (~2.70 Å).[30–32] The internal OH bond is also largely stretched to 1.04 from 0.98 Å for the gaseous dimer. One can thus infer that the H bond in the adsorbed dimer is largely enhanced, which can be confirmed again in the vibrational spectra analysis and isodensity contour plots given in Sec. IV. A wider ∠HOH in the donor and a narrower ∠HOH in the acceptor are also observed, which appears to be caused by electron transfer between water and the surface hydroxyls due to the H-bonding interactions. This enhancement of the H bonding in the adsorbed dimer is also observed on metal surfaces.[30–32] Finally, the two nonhydrogen-bonded surface hydroxyl groups, almost standing upright on the clean surface, are, however, reoriented towards the proton donor water accordingly to satisfy the H bonding between the adsorbed dimer and the substrate, as can also be observed for the monomer adsorption. These results will not be changed by doubling the surface cell in the calculations.

Another metastable configuration can be obtained (denoted as bridge2 in Table II), if the free OH bond in the adsorbed dimer orients to and is H bonded with its nearest hydroxyl group, and the OH bond of this hydroxyl directs away from the dimer at the same time and becomes free. This way, the number of HBs, which is still 5, is not changed. All OH bonds are participated in H-bonding interactions. However, this structure has deviated severely from the free dimer and therefore is less stable than the above configuration (by 98 meV per water molecule).

We studied water adsorption at 0.5 ML coverage by putting four water molecules in the doubled $\sqrt{2}\times\sqrt{2}$ surface cell. Only single gamma k point is used and the energy cutoff is reduced to 300 eV. The most favored structure among all the calculated configurations is presented in Fig. 3(a). Instead of a clustered structure, two separated dimers are formed there. The adsorption energy is 732 meV/H_2O and geometry parameters for each dimer are almost the same as those for dimer adsorption in the unit cell. Thus, the configuration of the adsorbed dimer in the unit surface cell is actually representing water adsorption at 0.5 ML in this sense. The only difference is the system sizes. The small energy difference between the two supercells (16 meV/H_2O), which

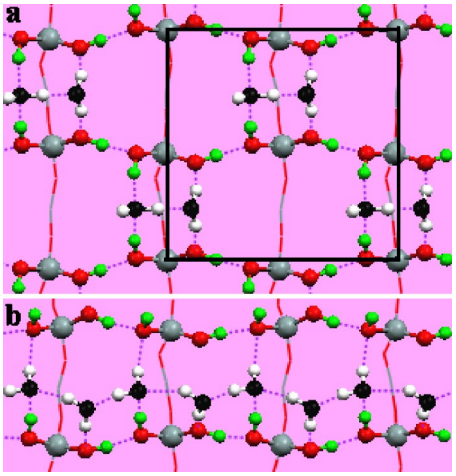

FIG. 3. (Color online) Water adsorption on β-cristobalite (100) at a half ML coverage for two different configurations, (a) isolated dimer domains and (b) water chains.

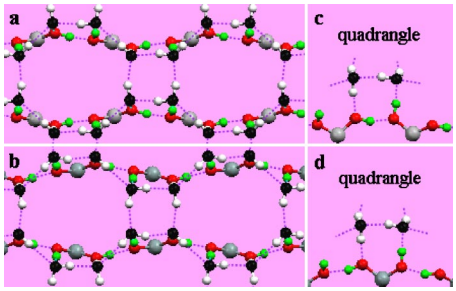

FIG. 4. (Color online) Tessellation ices on two different adsorption sites from the top view (a and b) and the side view (c and d), shown with the outmost layer of the substrate. To depict the adsorption sites clearly, only two water molecules of the quadrangle are shown in the side view panels.

is almost within the calculation accuracy, suggests the finite-size effect of the supercell is negligible.

Another interesting type of structure at 0.5 ML is one-dimensional (1D) water wire, formed between the two H-bond chains of surface hydroxyls [see Fig. 3(b)]. One OH bond of each water molecule connects another H_2O by a H bond, and the other OH bond is H bonded with the left (H-left) or the right (H-right) surface hydroxyl acting as a proton donor. A zigzag water wire is thus formed by connecting one H-left molecule and then another H-right molecule alternatively, bridging two adjacent H-bonded surface hydroxyl chains. Although all OH bonds in water are saturated with HBs here, it is less stable by about 100 meV/H_2O in adsorption energy than the most stable structure at 0.5 ML. We note that the two neighboring water wires on the hydroxylated β-cristobalite (100) surface cannot interact with each other directly, and hence could be useful for the anisotropic conductance of electrons or protons.

3. 2D tessellation ice on β-cristobalite (100)

Water forms an interesting 2D fully hydrogen-bonded water network consisting of quadrangular and octagonal rings of water molecules on the hydroxylated β-cristobalite (100) surface at 1 ML coverage (see Fig. 3 in Ref. 18). This interesting water pattern, named tessellation ice, was reported in our previous letter.[18] An obvious characteristic is strong H-bonding interactions inside the quadrangular water rings and weak H bonding between them. Each adsorbed water molecule in this phase is saturated with four H bonds, serving as a double proton donor and double proton acceptor. The adsorption energy of the tessellation ice on β-cristobalite (100) is large, 712 meV/H_2O, almost the same as adhesive energy in bulk ice, 720 meV.[34] More interestingly, this 2D ice structure is found to be stable up to room temperature (300 K).

In the tessellation ice, each hydroxyl group is H bonded with one water molecule nearly atop it, serving as a proton-donor or proton-acceptor (Fig. 4). However, the water molecules can deviate in pairs from the exact top sites, to the left or the right alternatively of the H-bond chain of the hydroxyl groups. The two pairs of molecules from the adjacent water chains then approach closer and interact with each other through H bonding. A H-bonded quadrangle of water is thus

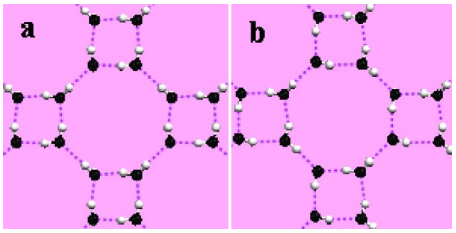

FIG. 5. (Color online) Ice tessellations with different proton orderings in (a) and (b).

formed. In fact, this quadrangle can sit over two different adsorption sites of the surface; i.e., the bridge site of two adjacent vicinal hydroxyl groups [Figs. 4(a) and 4(c)] and that of two adjacent geminal silanols [Figs. 4(b) and 4(d)]. There is only a slight difference (a few milli-electron volts) in energy between the two adstructures, indicating they are almost the same stable. Also, there exist two and only two possible types of proton ordering that can be present in a surface unit cell in the tessellation ice. One has anticlockwise dipoles in the water quadrangles [Fig. 5(a)], while the other type does not [Fig. 5(b)]. The former is less stable by $\sim$17 meV/H_2O. We believe that both proton orderings are possible in the tessellation ice. These two proton orderings in tessellation ice are meaningful only in the unit surface cell, and they will be more proton disordered if larger supercells are used. As a matter of fact, the disordered nature of proton distribution is common in ice structures according to the BFP ice rules,[35] such as in bulk ice *Ih*.

All these ice tessellations have many features in common whatever the proton ordering is, and wherever the quadrangular water ring sits. All H_2O molecules lie nearly coplanar on the surface. Two water molecules out of four in the unit cell lie nearly flatly on the surface by accepting a H bond each from surface hydroxyl groups, while the rest molecules have one OH bond pointing downward to the surface each and hence donating a H bond. In this way, every adsorbed water molecule is exactly H bonded to *three* neighboring molecules and a surface hydroxyl group, donating and accepting two protons simultaneously. Therefore, no free OH sticks out of the surface plane. The O-O distances of water molecules inside the quadrangles, 2.82–2.96 Å, are shorter than those connecting them, 3.16–3.30 Å, indicating strong H-bonding interactions inside and weak H bonding between the four-member water rings. At 1 ML coverage, it is the strongly H-bonded water quadrangle that serves as a bridge connecting the two adjacent parallel H-bond chains of hydroxyls on the surface.

We also investigated whether it is energetically feasible to add an additional water molecule inside the hole of the octagonal ring in the tessellation ice. We found that this molecule sits almost at the same level as those hydroxyls on the surface, and donates two weak H bonds to two hydroxyl groups (3.00 and 3.04 Å for O-O distances). However, its adsorption energy (referred to the system with adsorbed monolayer water) is 267 meV, which is hardly the half of that for the water monomer adsorption. More importantly, its participation does not distort the tessellation ice pattern at all and reduces the adsorption energy to 623 meV per molecule,

TABLE III. The optimized geometry parameters for water monomer, dimer, and monolayer adsorption on α-cristobalite (100). Energies, distances, and angles are in units of meV/H_2O, Å, and deg (°), respectively.

	E_{ads}	N_{HB}/H_2O	d_{OH1}	d_{OH2}	∠HOH	d_{OO}
Monomer	528	3	0.987	0.983	104.57	
Dimer	709	2.5	0.970	1.039	109.40	2.528
			0.994	0.991	107.27	
Tessellation ice	692	4	0.979	1.003	103.07	3.16,3.01,2.82
			0.990	0.994	106.60	
			0.992	0.984	109.45	
			0.999	0.984	104.56	

further proving the stability of the tessellation ice at the comparable coverage.

In order to examine the dependency of the ice tessellation structure on the silica surface, we optimized the geometry of a free layer of the tessellation ice. The result shows that the free tessellation layer is indeed a metastable structure, for it has a lower adhesion energy than the common hexagonal free ice bilayer (by 80 meV). What is more, it would contract to a smaller lattice constant and stronger H bonds, with two nonhydrogen-bonded OH bonds standing outside of the ice plane in a unit cell. Furthermore, the symmetry of the 2D ice layer is destroyed slightly. All these indicate that the existence of the present 2D quadrangular and octagonal ice structure is strongly dependent on the substrate. We conclude that the formation of the ice structure on the hydroxylated β-cristobalite (100) surface is mainly determined by the requirement of saturating hydrogen bonds among both water molecules and the surface hydroxyls. The highly directional surface hydroxyl groups and the quadrangular period in the silica surface also contribute to the emergence of the tessellation ice structure. The latter prohibits the formation of 2D hexagonal ice bilayer, which is generally observed on other single-crystal surfaces, such as Pt(111)[30,31] and Ru(0001).[36]

B. Water adsorption on α-cristobalite (100) surface

As a lower temperature phase of β-cristobalite, α-cristobalite has a structure of space group $P4_12_12$ and is more stable. Its (100) surface structure is very similar to that of β-cristobalite. The difference is that it has a smaller unit cell and contains only one Si atom in the unit cell in the surface layer. Thus the surface is more regular than β-cristobalite (100), at least in the respect that all the surface Si atoms are equivalent in it. However, the surface has to be rotated by 45° relative to β-cristobalite (100) to give the same direction of H-bond chains of the hydroxyls. The energy cutoff and k points used here are the same as those in the calculations of β-cristobalite (100). The adsorptive structures including water monomer, dimer, and monolayers, were also calculated. They all have the similar adsorption structure as their counterparts on β-cristobalite (100). The adsorption energies and the geometry data of these adstructures are tabulated in Table III.

Figure 6 compares the calculated adsorption energies for the most stable structures on the two surfaces: α- and β-cristobalite (100). They are plotted as functions of the different water coverage, such as 0.25 ML (monomer), 0.5 ML (dimer), and 1.0 ML (ice tessellation). It is striking that the same trends for water adsorption are found on both surfaces, though the adsorption energies on α-cristobalite (100) are always lower. On the both cristobalite (100) surfaces, the adsorption energy first increases and then decreases along the increase of coverage, showing a maximum at 0.5 ML coverage. From 0.5 to 1 ML coverage, the adsorption energy decreases only slightly by ~17 meV on both phases of substrate, indicating a weak exothermal procedure.

It is believed in literature that a crystalline silica surface could induce a more ordered water interface structure than an amorphous silica surface.[1] Recently, Ostroverkhov *et al.* have given the first evidence to confirm it, by finding an ice-like peak in their sum-frequency generation (SFG) spectra, resulted from the ordered and hydrogen-bonded OH bonds at the water/quartz (0001) surface.[3] This implies the tessellation ice structure could indeed exist on the cristobalite (100) surface, and on small domains of silica surface as well.

C. Water adsorption on β-cristobalite (111) surface

As mentioned in Sec. I, the β-cristobalite (111) surface, which sustains single isolated silanols identified on the silica surface by experiment, is another important surface to study.

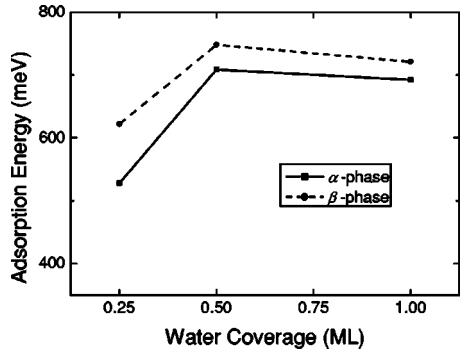

FIG. 6. The adsorption energy as a function of water coverage on α-cristobalite (100) (solid line) and β-cristobalite (100) (dashed line) surfaces. The coverages of 0.25 and 0.5 ML can only be viewed as pictorial, as they are used to model isolated monomers and dimers respectively at zero coverage.

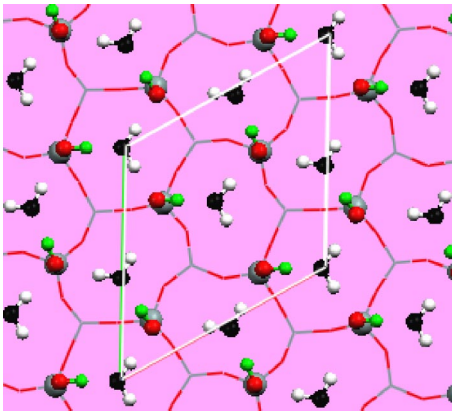

FIG. 7. (Color online) Water adsorption on the β-cristobalite (111) surface at 1 ML coverage.

It differs from the $\beta(\alpha)$-cristobalite (100) surface in two aspects: (i) It has a hexagonal periodicity other than rectangular in cristobalite (100). (ii) It supports the single silanols rather than geminal ones. A prominent feature of these silanols is that the distance between the two adjacent silanols is almost 5.0 Å, and thus they are isolated from interacting with each other. Hence different from the (100) surfaces, no H bond presents between surface hydroxyls on β-cristobalite (111). This is consistent with other works, for instance in Ref. 16. For the single, isolated silanol hydroxyl group on β-cristobalite (111), the bond angle of Si–O–H is about 120°, with the Si–O bond perpendicular to the surface and the O–H bond tilted by 60° from the surface normal. The hydroxyl group can rotate nearly freely around the Si–O axis without much difference in total energies, as also proposed by Peri[37] and confirmed by ^{29}Si CP-MAS nuclear magnetic resonance (NMR) studies[38] and quantum chemical calculations.[39] Therefore, we present just one of the surfaces with typical silanol orientations as an example in Fig. 7.

Water monomer adsorption has been calculated on the top site, the bridge site (between two adjacent silanols), and the hollow site. The hollow site is found to be the most favorable adsorption site. The adsorption energy is as large as 768 meV/H_2O for the water molecule on certain hollow sites, with the formation of three H bonds to the surface hydroxyls (O$\cdots$H lengths 1.676, 1.858, and 2.035 Å, respectively). The water thus serves as a double proton-donor and a proton-acceptor. Summarizing water molecule adsorption on both the cristobalite (100) and (111) surfaces, we note that the strength of water-silica bonds, which comprises mainly several hydrogen bonds, is usually larger than that on metal surfaces [such as 304 meV on Pt (111)[31] and 180 meV on Ag (111)],[40] salts (330 meV),[40] and some oxides [such as 555 meV on MgO (100)].[42]

For the monolayer adsorption on β-cristobalite (111), the orientation of the isolated single silanols becomes very important. Of all possible Si-OH orientations, only that shown in Fig. 7 can accommodate as many as four water molecules in the surface cell, where the maximum number of H bonds is reached. The optimized configuration is displayed in Fig. 7. The adsorption energy is 701 meV/H_2O for this adstructure. Each water molecule sits on the hollow site as the isolated monomer. However, there are some small differences in the circumstance of each hollow site in the monolayer adsorption, due to the slight differences between the surface Si atoms, just as that in the (100) surface. Therefore, some water molecules form three H-bonds as the monomer, while the others form only two H bonds with the hydroxyls, for the OO distance is too large to have any effective H-bonding in the third directional OH pointing ($d_{OO} > 3.60$ Å). As it is obviously seen that no H bonding interaction occurs between any two water molecules, and no tessellation-icelike water can be formed on this surface at 1 ML, which is substantially different from that on (100) surfaces. In fact, it is also different from the other hexagonal surfaces, for example of closely packed metal surfaces, on which ice bilayers are usually formed.[30,31,36] This is because the periodicity of the closely-packed metal $\sqrt{3}\times\sqrt{3}$ surfaces resembles that of ice (only expand to a few percent), while we have a much larger hexagonal period on the β-cristobalite (111) surface relative to dimensions of an ice surface *Ih*(0001) ($\sim$10.20 vs 4.52 Å). Accompanied by the quadrangular periodicity on cristobalite (100), this difference prevents the existence of ice bilayers on silica surface.

IV. VIBRATIONAL ANALYSIS

In general, the interwater hydrogen bonding at surfaces is strongly entangled with the water-surface interactions, especially on the hydroxylated surfaces, where water binds to the surfaces also through hydrogen bonds. Therefore the identification of these two interactions is important, though difficult. However, the OH stretches, which are sensitive to subtle structure modifications by surfaces and interfaces, can provide an effective approach for this purpose.[30] Moreover, they are usually easy accessible by experiments. Here we analyze the vibrations in the adsorbed water structures on hydroxylated silica surfaces, by calculating the vibrational spectra through MD simulations for typically 3–4 ps. The vibrational data can also provide a database for future experimental studies.

We have calculated the vibrational spectra for the water monomer, dimer, and ice tessellation on the β-cristobalite (100) surface, and the water monolayer on β-cristobalite (111). The eigenfrequencies for the adsorbed structures and the free water monomer and dimer are listed in Table IV. It is easy to see the good agreement between theory and experiment[43–45] (see Table IV). Thus we can summarize the method we used here is good enough to get the vibrational spectra. These spectra are generally dominated by three regions: the low-frequency region below 140 meV for the intermolecular translations and librations, the HOH bending mode around 200 meV, and the high-frequency intramolecular OH stretches between 347 and 478 meV (one exception is the OH stretch at 284 meV in the adsorbed dimer). The hydrogen bonding always exhibits a redshift in the involved OH bond stretching. The larger redshift arises from the longer OH bond, and the shorter intermolecular O-O distance, which indicates the stronger H bond is formed.

An extreme case is the H bond in the adsorbed dimer on β-cristobalite (100) surface. A peak located at 284 meV,

TABLE IV. Calculated vibrational energies (in meV) for the water monomer, dimer, and tessellation ice on β-cristobalite (100), and 1 ML on β-cristobalite (111). The last four rows list the theoretical and experimental values for a gaseous water molecule and dimer for comparison. The $\nu_{\text{O-Hw}}$ represents OH stretch energies for the H bonds between water molecules. Other OH [coming from surface silanols (Si-OH) or water] vibrations are denoted as $\nu_{\text{O-H}}$. The δ_{HOH} is HOH bending mode.

	Translations and librations						δ_{HOH}	$\nu_{\text{O-Hw}}$	$\nu_{\text{O-H}}$
Monomer/β(100)	14	30	47	64	72	102	200		444,478
Dimer/β(100)	19		53	69	81	109	197	284	414,428,476
Ice/β(100)	12	28	55	69	77	97,109	202	406,428,456	347,378
1 ML/β(111)	10	40	59	75	89	105	202		422,432
									448,475
H_2O							198		462,478
H_2O (expt.)[a]							198		454,466
Dimer	20	34	46	67			198	442	462,473,483
Dimer (expt.)[b]	19[c]	30[c]	40[c]	65[c]			201	440	450,459,461

[a]Reference 43.
[b]Reference 44.
[c]Reference 45.

which is apparently not in the earlier three regions, is salient in the vibrational spectrum for the dimer. We assign this peak to the H-bonded OH stretching mode between the two H_2O in the dimer. This assignment can be justified by tracing the trajectory of the bridging OH bond length from a 4000 fs MD simulation, as shown in Fig. 8(a). The averaged OH bond length (1.05 Å) is much longer than that in a free dimer (0.984 Å, calculated). Fourier transform of the OH curve in Fig. 8(a) yields a vibrational energy at 284 meV (see the inset). This vibration energy undergoes a much larger shift, compared to that in the free dimer (440 meV)[44] and in the normal ice *Ih* (390 and 403 meV).[35] Moreover, the averaged O-O distance of 2.515 Å in the MD simulation [Fig. 8(b)] agrees reasonably well with that obtained in our static geometry calculations (2.530 Å). It is much shorter than that for a free water dimer (2.895 Å, calculated). All above data on the OH bond and O-O separations indicate the adsorbed dimer on the β-cristobalite (100) surface comprises a strong H bond, which mainly comes from the perfect fitting of the geometry of water dimer to the structural restriction of the substrate.

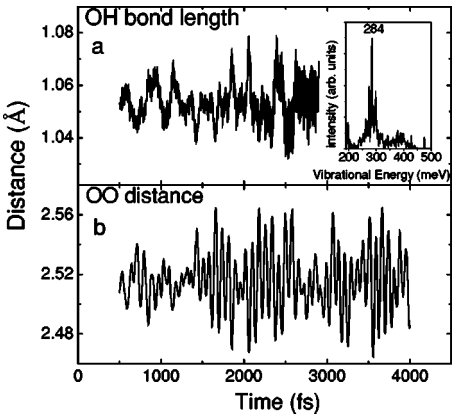

FIG. 8. The variation of (a) the bridging OH bond length and (b) the OO distance versus simulation time, recorded in a 3500 fs MD simulation of the water dimer adsorbed on the hydroxylated β-cristobalite (100) surface. The inset in (a) shows the Fourier transform of the OH bond length curve (vibrational spectrum).

Two types of H bonds in different strength in the tessellation ice can be identified from the vibrational spectrum.[18] One is the strong H bond inside the quadrangles, as indicated by 406 and 428 meV modes, and the other is the weak H bond between the two neighboring quadrangles, indicated by 456 meV mode. Our assignment of these two kinds of H bonds is justified by tracing the trajectories of the OH bond lengths in the MD simulation shown in Fig. 9. The OH bond length variations for such a strong and weak H bond are plotted as a function of simulation time. Both OH bond lengths are longer than that of a free H_2O molecule (0.973 Å, calculated), and the strong H bond has even longer OH bond lengths and a lower vibrational frequency. While the two lowest vibrational energies of the OH stretching modes 347 and 378 meV come from the vertical H bonds formed by the surface hydroxyl (Si-OH). Thus the separation between the OH stretching modes of the ice plane and the surface hydroxyl groups can be clearly seen. Although the H bonds in the ice plane are entangled with those between wa-

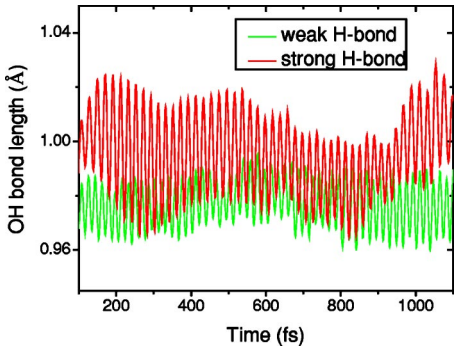

FIG. 9. (Color online) The variation of OH bond length involved in the strong and the weak H bonds vs time in a 1000 fs MD simulation of the tessellation ice on β-cristobalite (100).

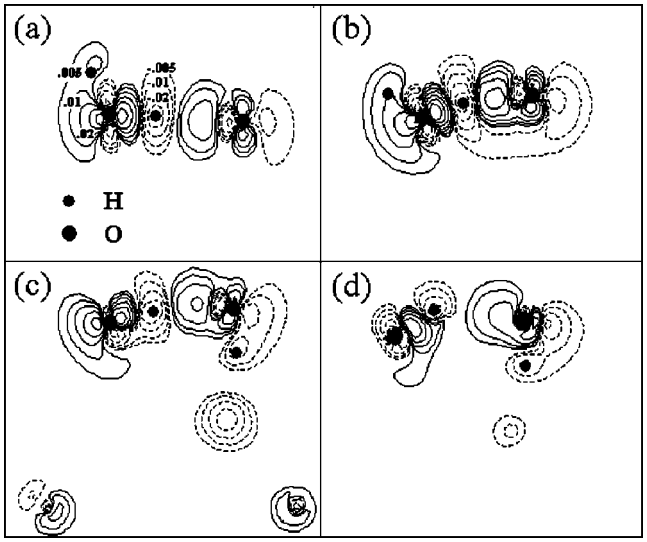

FIG. 10. Isodensity contour plots of the difference electron density for (a) the free water dimer, (b) the adsorbed dimer on β-cristobalite (100), (c) the strong H bonds, and (d) the weak H bonds in the tessellation ice. The difference density is defined as $\Delta\rho=\rho[(H_2O)_2]-\rho[H_2O_{(1)}]-\rho[H_2O_{(2)}]$ for a free dimer, $\Delta\rho=\rho[(H_2O)_2/SiO_2]-\rho[H_2O_{(1)}/SiO_2]-\rho[H_2O_{(2)}/SiO_2]+\rho[SiO_2]$ for the adsorbed dimer, and $\Delta\rho=\rho[(H_2O)_{total}/SiO_2]-\rho[(H_2O)_1+enviroment)/SiO_2]-\rho[(H_2O)_2+enviroment)SiO_2]+\rho[environment/SiO_2]$ for H bonds in tessellation ice. The contours have densities of $\Delta\rho=\pm0.005\times2^k$ e/Å^3, for $k=0,1,2,3\ldots,6$ and the first three values are marked in (a) for instance. Solid and dashed lines correspond to $\Delta\rho>0$ and $\Delta\rho<0$, respectively. The positions of oxygen and hydrogen atoms are also depicted by large and small black balls, respectively.

ter and the surface hydroxyls inevitably, the vibrational spectrum presented here can provide a means for distinguishing them from each other.

For the monolayer water on the hydroxylated β-cristobalite (111) surface, the OH stretch modes calculated from a 2000 fs MD simulation at 80 K are located at 422, 432, 448, and 475 meV. The 475 meV mode is very close to the free OH stretch mode in energy (476 meV), suggesting there is an almost free OH bond in the water monolayer, in agreement with our analysis from the static calculations (Fig. 7). Due to the different circumstances for each OH in the surface cell, the H bonds formed by the hydroxyls are different in strength, as implied by the frequencies of 422, 432, and 448 meV, respectively.

The nature of the intermolecular H bond in the free dimer, adsorbed dimer, and tessellation ice on the hydroxylated β-cristobalite (100) surface can be displayed by the isodensity contour plots of the difference charge density, as shown in Fig. 10. The horizontal axis goes along the O-H$\cdots$O bond, while the vertical axis lies in the surface normal. For the free dimer [Fig. 10(a)], formation of the H bond leads to electron transfer from the proton donor (the left molecule) to the acceptor (the right molecule) in the bonding region. The greatly enhanced charge redistribution for an adsorbed dimer in Fig. 10(b) confirms once again that the H bond is strengthened upon adsorption. For the strong H bond in the tessellation ice [Fig. 10(c)], the charge redistribution is also obvious, and has a similar intensity as in the free dimer. However, the charge redistribution is less significant for the weak H bond in the 2D ice [Fig. 10(d)]. This difference justifies our prediction of two types of H bonds in the tessellation ice: the strong H bonds in the water quadrangles and the weak H bonds between them.

V. SUMMARY

We have systematically studied the interaction between water and the hydroxylated cristobalite (100) and (111) surfaces using the density-functional total-energy calculations within the generalized gradient approximation. These two single-crystal surfaces can support the two surface silanol configurations observed in experiment: the geminal and single silanols, and hence, represent prototype silica surface domains for general understanding of water-silica interactions. A series of water adsorbates ranging from monomers to monolayers have been investigated, and general features and trends were found.

(1) The water-silica bond consists simply of several hydrogen bonds between water and surface hydroxyls in nature. However, this water-silica binding is usually stronger than the general water-surface bonds for molecular water adsorption on other surfaces, such as closely packed metal surfaces (with energy of 100–400 meV),[31,40] salts (330 meV),[41] and some oxide surfaces ($\sim$550 meV).[42] This is true for water monomer adsorption on the β-cristobalite (100) (adsorption energy 622 meV), α-cristobalite (100) (528 meV), and β-cristobalite (111) (768 meV) surfaces, and three H bonds form between the water and the surface in each case. The same nature of water-silica bonds applies also to water clusters (like the dimer) and monolayer adsorption (like the tessellation ice).

(2) Because of the same H-bond interaction in the water-silica bonds and interwater interactions, water forms into a number of different adsorption structures on all the investigated surfaces, such as stabilized monomers, isolated clusters, 1D chains, and monolayers. These structures have varied stability and are unique on the specialized surfaces. Prominent examples include the tessellation ice with characteristic quadrangular and octagonal water rings on cristobalite (100), and isolated water molecules, H bonded to surface hydroxyls, in a monolayer on cristobalite (111). Another example is the greatly enhanced hydrogen bonding in the adsorbed dimer due to the geometrical fixation on the substrate. Of the studied water species, the water dimer has the maximum adsorption energy.

(3) Therefore it could be important to distinguish the water-surface bonds and interwater interactions, due to the identical nature of these two interactions for water adsorption on silica surface. Although the two interactions entangle with each other and could be more complicated in a real case, we fortunately observed that surface OH stretches usually have a clear separation from those between water molecules, which provides a means to distinguish between surface hydroxyls and OH groups in water. For example, a lower OH vibration frequency (350–380 meV) was observed for water-surface bonds due to stronger

Si–OH$\cdots$OH$_2$ in the tessellation ice, while the interwater OH modes are located at 400–460 meV. For a water dimer adsorbed on β-cristobalite (100), however, the interwater H bond exhibits a much lower OH mode at 284 meV, which is again far from OH modes in water-silica H bonds (410–430 meV). Similar vibration recognition techniques of surface water have already been developed on the metal surfaces.[31]

(4) Covered by geminal and vicinally H-bonding hydroxyl groups, β- and α-cristobalite (100) display very similar properties as regards water adsorption. Very similar behaviors were observed for water monomer, half-monolayer, and monolayer adsorption on both surfaces. The adsorption energy on α-cristobalite (100) is always lower than that on β-phase, but exhibits the same trend with an increase of water coverage. A 2D ice phase, tessellation ice with characteristic quadrangular and octagonal rings of water molecules, is formed on the both (100) surfaces at 1 ML coverage. In the tessellation ice, the quadrangular water rings sit either on the bridge of two geminal sites or vicinal sites. It also shows two typical different proton-orderings within our surface cell. However, very different water adsorptive behaviors have been found on the cristobalite (111) surfaces. As it sustains another important type of silanols found on silica—single silanols, the β-cristobalite (111) surface displays completely different adsorptive structures upon water adsorption from those adstructures on the (100) surface. A hydrogen bond is neither formed between any two isolated hydroxyls, nor formed between any two water molecules at 1 ML coverage on β-cristobalite (111). Therefore, only isolated water molecules, but no icelike water is formed on this surface, which is totally different from the case of cristobalite (100).

(5) Compared with water adsorption on other common surfaces, such as on metal surfaces, water on silica can behave both similarly and substantially differently. Similar structures in the adsorbed water dimer and 1D chains are found on cristobalite (100) surfaces and on Pt(111).[31] Enhanced H bonding in the adsorbed dimer shows up in both cases. Furthermore, two types of hydrogen bonds of different strengths are determined in the 2D connected water networks at monolayer coverages on both cristobalite (100) and metal surfaces. However, there are still significant differences between water adsorption on the two categories of surfaces. First, much more enhanced H bonding in the adsorbed dimer is observed on cristobalite (100) than on metals, which can be indicated from the H bond length (more shortened), the vibrational spectra from MD simulations (more redshifted OH modes), and the redistribution of the charge between the dimer (more enhanced). The possible reason for this large enhancement may be the perfect fit between the structure of the cristobalite substrate and the geometry of water dimer. Second, the partition of the two types of H bonds in hydrogen-bonded networks originates differently. It comes from the connection of different water network patterns on cristobalite (100), but results from the different numbers of H bonds water donates on metal surfaces. Finally and most importantly, the ice tessellation made of quadrangular and octagonal patterns of water molecules forms on cristobalite (100) and isolated water molecules on β-cristobalite (111) at ML coverage, while an ice *Ih*-like hexagonal water bilayer forms on closely packed metal surfaces. The ice tessellation phase is highly dependent on the surface structure of the substrate. Its formation is mainly determined by the requirement of saturating hydrogen bonds among water molecules. The cristobalite (100) surface with geminal hydroxyls, which provide active sites by either donating or accepting H bonds, satisfies this requirement perfectly, while the hexagonal metal surfaces match the tessellation ice poorly. Although few experimental data are available so far on the cristobalite surfaces studied, we believe our predicted tessellation ice indeed exists and even on the small domains of the silica surface. In fact, evidence for the ordered hydrogen-bonded water network on the crystal silica surface has already been provided by a recent experiment.[3]

ACKNOWLEDGMENTS

We thank Mike Dotson for his critical reading of this manuscript. This work has been supported by the NSF and MOST of China.

*Author to whom correspondence should be addressed. Email address: egwang@aphy.iphy.ac.cn

[1] *The Chemistry of Silica*, edited by R. K. Iler (Wiley, New York, 1979), Chap. 6.

[2] *The Surface Properties of Silica*, edited by A. P. Legrand (Wiley, New York, 1998).

[3] Q. Du, E. Freysz, and Y. R. Shen, Phys. Rev. Lett. **72**, 238 (1994); V. Ostroverkhov, G. A. Waychunas, and Y. R. Shen, Chem. Phys. Lett. **386**, 144 (2004).

[4] B. Fubini, V. Bolis, M. Bailes, and F. S. Stone, Solid State Ionics **32**, 258 (1989).

[5] O. Sneh and S. M. George, J. Phys. Chem. **99**, 4639 (1995); O. Sneh, M. A. Cameron, and S. M. George, Surf. Sci. **364**, 61 (1996).

[6] A. Burneau, O. Barrès, J. P. Gallas, and J. C. Lavalley, Langmuir **6**, 1364 (1990).

[7] J. H. Anderson and K. A. Wickersheim, Surf. Sci. **2**, 252 (1964).

[8] K. Klier, J. Chem. Phys. **58**, 737 (1973).

[9] K. Klier, J. H. Shen, and A. C. Zettlemoyer, J. Phys. Chem. **77**, 1458 (1973).

[10] A. M. Ferrari, P. Ugliengo, and E. Garrone, J. Phys. Chem. **97**, 2671 (1993).

[11] A. G. Pelmenschikov, G. Morosi, and A. Gamba, J. Phys. Chem. A **101**, 1178 (1997); J. Phys. Chem. **96**, 7422 (1992).

[12] D. A. Litton and S. H. Garofalini, J. Non-Cryst. Solids **217**, 250 (1997).

[13] N. H. de Leeuw, F. M. Higgins, and S. C. Parker, J. Phys. Chem. B **103**, 1270 (1999).

[14] I.-S. Chuang and G. E. Maciel, J. Phys. Chem. B **101**, 3052 (1997); J. Am. Chem. Soc. **118**, 401 (1996).

[15] S. Iarlori, D. Ceresoli, M. Bernasconi, D. Donadio, and M. Parrinello, J. Phys. Chem. B **105**, 8007 (2001).
[16] D. Ceresoli, M. Bernasconi, S. Iarlori, M. Parrinello, and E. Tosatti, Phys. Rev. Lett. **84**, 3887 (2000).
[17] F. Vigné-Maeder and P. Sautet, J. Phys. Chem. B **101**, 8197 (1997).
[18] J. Yang, S. Meng, L. F. Xu, and E. G. Wang, Phys. Rev. Lett. **92**, 146102 (2004).
[19] G. Kresse and J. Hafner, Phys. Rev. B **47**, 558 (1993); **49**, 14251 (1994); J. Phys.: Condens. Matter **6**, 8245 (1994); G. Kresse and J. Furthmüller, Comput. Mater. Sci. **6**, 15 (1996); Phys. Rev. B **54**, 11 169 (1996).
[20] R. Jones and O. Gunnarsson, Rev. Mod. Phys. **61**, 689 (1989); M. Payne, M. Teter, D. Allan, T. Arias, and J. Joannopoulos, *ibid.* **64**, 1045 (1992); M. Gillan, Contemp. Phys. **38**, 115 (1997).
[21] J. P. Perdew, J. A. Chevary, S. H. Vosko, K. A. Jackson, M. R. Pederson, D. J. Singh, and C. Fiolhais, Phys. Rev. B **46**, 6671 (1992); Y. Wang and J. P. Perdew, *ibid.* **44**, 13298 (1991).
[22] J. Goniakowski and M. J. Gillan, Surf. Sci. **350**, 145 (1996).
[23] N. H. de Leeuw and J. A. Purton, Phys. Rev. B **63**, 195417 (2001).
[24] L. Giordano, J. Goniakowski, and J. Suzanne, Phys. Rev. Lett. **81**, 1271 (1998).
[25] S. Tsuzuki and H. P. Lüthi, J. Chem. Phys. **114**, 3949 (2001).
[26] D. Vanderbilt, Phys. Rev. B **41**, 7892 (1990).
[27] H. J. Monkhorst and J. D. Pack, Phys. Rev. B **13**, 5188 (1976).
[28] A. F. Wright and A. J. Leadbetter, Philos. Mag. **31**, 1391 (1975).
[29] F. Liu, S. H. Garofalini, R. D. King-Smith, and D. Vanderbilt, Phys. Rev. Lett. **70**, 2750 (1993).
[30] S. Meng, L. F. Xu, E. G. Wang, and S. Gao, Phys. Rev. Lett. **89**, 176104 (2002); **91**, 059602 (2003).
[31] S. Meng, E. G. Wang, and S. Gao, Phys. Rev. B **69**, 195404 (2004).
[32] V. A. Ranea, A. Michaelides, R. Ramírez, P. L. de Andres, J. A. Vergés, and D. A. King, Phys. Rev. Lett. **92**, 136104 (2004).
[33] T. R. Dyke, K. M. Mack, and J. S. Muenter, J. Chem. Phys. **66**, 498 (1977).
[34] P. J. Feibelman, Phys. Rev. B **67**, 035420 (2003).
[35] P. A. Thiel and T. E. Madey, Surf. Sci. Rep. **7**, 211 (1987); M. A. Henderson, *ibid.* **46**, 1 (2002).
[36] P. J. Feibelman, Science **295**, 99 (2002); D. Menzel, *ibid.* **295**, 58 (2002).
[37] J. B. Peri, J. Phys. Chem. **70**, 2937 (1966).
[38] I.-S. Chuang, D. R. Kinney, and G. E. Maciel, J. Am. Chem. Soc. **115**, 8695 (1993).
[39] J. Sauer, Chem. Phys. Lett. **97**, 275 (1983).
[40] V. A. Ranea, A. Michaelides, R. Ramírez, J. A. Vergés, P. L. de Andres, and D. A. King, Phys. Rev. B **69**, 205411 (2004).
[41] J. M. Park, J.-H. Cho, and K. S. Kim, Phys. Rev. B **69**, 233403 (2004).
[42] D. Ferry, S. Picaud, P. N. M. Hoang, C. Girardet, L. Giordano, B. Demirdjian, and J. Suzanne, Surf. Sci. **409**, 101 (1998).
[43] K. Kuchitsu and Y. Morino, Bull. Chem. Soc. Jpn. **38**, 805 (1965).
[44] A. J. Tursi and E. R. Nixon, J. Chem. Phys. **52**, 1521 (1970).
[45] R. M. Bentwood, A. J. Barnes, and W. J. Orville-Thomas, J. Mol. Spectrosc. **84**, 391 (1980).